www.sciencemag.org/content/361/6401/502/suppl/DC1

Supplementary Materials for

HAIRY MERISTEM with WUSCHEL confines CLAVATA3 expression to the outer apical meristem layers

Yun Zhou*†, An Yan*, Han Han, Ting Li, Yuan Geng, Xing Liu, Elliot M. Meyerowitz†

*These authors contributed equally to this work.
†Corresponding author. Email: meyerow@caltech.edu (E.M.M.); zhouyun@purdue.edu (Y.Z.)

Published 3 August 2018, *Science* **361**, 502 (2018)
DOI: 10.1126/science.aar8638

This PDF file includes:

Other Supplementary Material for this manuscript includes the following:
(available at www.sciencemag.org/content/361/6401/502/suppl/DC1)

Materials and Methods

Computational modeling and simulation

The computational model for the SAM is simulated on a dome-shaped template represented as 1216 overlapping spheres, which roughly mimics the SAM of *Arabidopsis*. For simulation of the axillary meristem (AM), the dome-shaped template was downsized to 446 overlapping spheres, to mimic the smaller size of initiating meristems. Cell positions are specified by 3D spatial coordinates, and cell sizes are specified by the radius of each sphere. Cell neighbors are found by searching for overlapping spheres. For *WUS* activation, a rib zone-localized OC signal is initially defined manually. The experimentally determined *HAM* expression patterns in wild type and different genetic perturbations were used as inputs for the SAM computational model. For wild type and different genetic perturbations, different HAM protein localization patterns were specified based on experimental confocal microscope observations of reporter lines. Different HAM expression patterns in various stages of wild type AM development were based on *HAM* RNA *in situ* hybridization experiments, and then used as inputs for simulation of gene expression pattern formation process in AM development. For AM initiation simulation, OC signal was defined as shown in Fig. S10. Dynamics of 4 key molecules, namely *WUS* mRNA ([WUSr]), WUS protein ([WUSp]), *CLV3* mRNA ([CLV3r]), and CLV3 peptide ([CLV3p]) are described using the system of differential equations that are listed below. The equations are applicable to each of the cells in the template, the cell indices are omitted in the equations as shown.

$$\frac{d[WUSr]}{dt} = k_{wrp}[OCSignal]\left(1 - \frac{[WUSr]}{[WUSr]_{max}}\right) - k_{wrn}[WUSr](\gamma_{WUSr} + [CLV3p]) \quad \ldots\ldots\ldots\ldots\ldots\ldots (1)$$

Equation (1) describes the dynamics of *WUS* mRNA levels. k_{wrp} is the parameter for *WUS* mRNA production. *WUS* mRNA production is activated by a rib meristem signal and is saturated by a maximum *WUS* mRNA value $[WUSr]_{max}$. For degradation of *WUS* mRNA, we introduced both CLV3-dependent and independent down-regulation terms. k_{wrn} is the general parameter for *WUS* mRNA degradation and γ_{WUSr} is the parameter for CLV3-independent *WUS* mRNA degradation.

$$\frac{d[WUSp]}{dt} = k_{wpp}[WUSr] - k_{wpn}[WUSp] + D_{WUSp}\Delta[WUSp] \quad \ldots\ldots\ldots\ldots\ldots\ldots\ldots\ldots\ldots\ldots\ldots\ldots\ldots\ldots\ldots\ldots\ldots\ldots\ldots\ldots (2)$$

Equation (2) describes the dynamics of the WUS protein. k_{wpp} is the parameter for WUS protein translation from *WUS* mRNA. k_{wpn} is the parameter for WUS protein degradation. D_{WUSp} is the passive diffusion-like symplastic transport constant of WUS protein. The unit for the WUS transport constant in the model is "average common cell surface area between two neighboring cells (in arbitrary unit of area)/time hour". The diffusion of WUS protein happens via plasmodesmata between cells in SAMs, which is only a small portion of the cell wall area. So the effective apparent diffusion constant for WUS protein used in this model cannot be directly compared to the protein diffusion constant in liquid solutions or cell cytosol.

$$\frac{d[CLV3r]}{dt} = k_{crp}[WUSp](1 - [HAMp])\left(1 - \frac{[CLV3r]}{[CLV3r]_{max}}\right) - k_{crn}[CLV3r] \dots\dots\dots\dots\dots\dots\dots\dots..\dots.\dots(3)$$

Equation (3) describes dynamics of *CLV3* mRNA. k_{crp} is the parameter for *CLV3* mRNA production. *CLV3* mRNA production is activated by WUS protein, inhibited by HAM proteins, and saturated at a maximum *CLV3* mRNA value $[CLV3r]_{max}$. k_{crn} is the parameter for *CLV3* mRNA degradation.

$$\frac{d[CLV3p]}{dt} = k_{cpp}[CLV3r_{effective}] - k_{cpn}[CLV3p] + D_{CLV3p}\Delta[CLV3p] \dots\dots\dots\dots\dots\dots.\dots\dots\dots.\dots\dots\dots..(4)$$

Equation (4) describes the dynamics of the apoplastic movement of the secreted CLV3 peptide. k_{cpp} is the parameter for CLV3 peptide formation from *CLV3* mRNA. A term called $[CLV3r_{effective}]$ describes the buffered *CLV3* mRNA level. k_{cpn} is the parameter for CLV3 peptide degradation. D_{CLV3p} is the passive diffusion-like apoplastic transport constant of CLV3 peptide. The movement of CLV3 peptide can be the combined result of exocytosis from all parts of the plasma membrane, and apoplastic diffusion. Therefore, we assumed a relative faster apparent diffusion constant for CLV3 peptide compared to WUS protein.

$$[CLV3r_{effective}] = \begin{cases} [CLV3r] & [CLV3r] \le C_{bufferlow} \\ C_{bufferlow} & C_{bufferlow} < [CLV3r] < C_{bufferhigh} \\ [CLV3r] - C_{bufferhigh} + C_{bufferlow} & [CLV3r] \ge C_{bufferhigh} \end{cases} \quad \dots..(5)$$

Equation (5) describes the buffered *CLV3* mRNA phenomenon (21). Based on a previous report that *CLV3* mRNA level can be varied in a ten-fold range without affecting *WUS* RNA level and SAM development *(19),* we introduced a stepwise linear function to consider the "effective" buffered *CLV3* mRNA levels.

$C_{bufferlow}$ and $C_{bufferhigh}$ are the parameters for low and high thresholds of the buffered range of *CLV3* mRNA, respectively. A biological mechanism for CLV3 activity level buffering is suggested in *(8)*.

Simulations were carried out using the explicit forward Euler method with fine fixed time steps. Wild type SAM was simulated using parameter values given in Table S1. To simulate the SAM of *Mir171OE*, HAM input was set to 40% of the WT control level based on the experimental result (Fig. S6C). To simulate the SAM of the *ham1;2;3* mutant, HAM input was set to zero. To simulate the SAM of the *wus-1* null mutant, parameter for *WUS* mRNA production rate (k_{wrp}) was set to zero. To simulate the SAM of the *wus-7* partial loss of function mutant, the activity of WUS protein to activate *CLV3* mRNA production (k_{crp}) was set to 5% of the WT control level. The above described parameter changes were combined for simulations of the SAMs in *wus-1;ham1;2;3* and *wus-7;ham1;2;3* mutants.

In addition, as negative simulation controls, we modified Equation (3) by assuming HAM to be a positive regulator of *CLV3* mRNA production either by itself or synergistically with WUS protein. Predictions of *CLV3* mRNA expression patterns by these alternative

models do not match the experimentally derived *CLV3* transcript pattern, as shown in Fig. S3. In Fig. S3, we altered the relation of HAM and WUS in two different ways, the equations for Fig. S3A and Fig. S3B were:

$$\frac{d[CLV3r]}{dt} = k_{crp}[WUSp][HAMp]\left(1 - \frac{[CLV3r]}{[CLV3r]_{max}}\right) - k_{crn}[CLV3r] \ldots\ldots\ldots\ldots\ldots\ldots\ldots (S3A)$$

$$\frac{d[CLV3r]}{dt} = k_{crp}[WUSp](1 + [HAMp])\left(1 - \frac{[CLV3r]}{[CLV3r]_{max}}\right) - k_{crn}[CLV3r] \ldots\ldots\ldots\ldots\ldots (S3B)$$

Equation S3A assumes that WUS and HAM work together to activate the production of *CLV3* mRNA (both HAM and WUS are required for activation). Equation S3B assumes that HAM activates CLV3 mRNA production in addition to WUS. When we replaced equation 3 with either equation S3A or equation S3B in the model, we found that in these two scenarios, the simulated *CLV3* mRNA patterns (Fig. S3) are greatly different from the experimentally observed *CLV3* mRNA pattern in a wild type SAM.

To further test the SAM model in the presence of dynamic template perturbations due to cell growth and divisions, we introduced growth and divisions into our simulation template. In the dynamic SAM template, cells move away from center of the SAM laterally to mimic cell growth and cell division as it occurs in the meristem *(27)*. The asynchronous division of cells is randomly decided. In the center of the SAM, cells divide more slowly, while cells in the peripheral zone divide more rapidly, to meet the constraint of stable meristem shape. Simulation using this dynamic template shows that the gene expression patterns in SAM are stable in the presence of cell growth and division (Movies S4-S6).

For one additional special model reduction test, we simplified the 3D SAM template into a 1-D cell layer-based template. Since L1, L2 and corpus are distinct clonal layers in the shoot apex, which are undisturbed by cell growth and divisions, a further simplified 1D+t cell layer model can also produce the apical-basal gradients of *WUS* and *CLV3* transcripts (Movie S7).

Plant materials and growth conditions

The *pHAM1::2xYPET-N7MirS*; *pCLV3::TFP-ER* double-reporter plant was generated through genetic crossing between *pHAM1::2xYPET-N7MirS (15)* and *pCLV3::TFP-ER (28)*. The *pHAM2::YPET-HAM2*; *pCLV3::TFP-ER* double reporter was generated through genetic crosses between *pCLV3::TFP-ER* and the *HAM2* translational reporter *pHAM2::YPET-HAM2* that was previously described *(15)*. *pCLV3::DsRed-N7* was reported previously *(14)* and the *pATML1::HAM1m-GFP*; *pCLV3::DsRed-N7* plant was generated through the transformation of the plasmid harboring *pATML1::HAM1m-GFP* into *pCLV3::DsRed-N7*(L*er*) through floral dip *(29)*. The binary vector containing the *ATML1* promoter was previously published *(30)*. The microRNA171-insensitive version of HAM1 (here referred as HAM1m) was used in *pATML1::HAM1m-GFP*, with the mutated Mir171 recognition sites as described previously *(18)*. The *Mir171OE* transgenic plants were generated through floral dip transformation of a pMDC32 *35S::Mir171*

vector into the L*er* wild type which contains a *pWUS::DsRed-N7* reporter. *ham1;2;3* was backcrossed to L*er*, and the genotyping and generation of *wus-7*, *wus-7;ham1;2;3* quadruple mutant, *wus-1*, *wus-1;ham1;2;3* quadruple mutant was done as described previously *(15).*

qPCR

The levels of gene expression in both wild-type controls and the *Mir171OE* transgenic plants were quantified through the real-time RT-PCR. The plants from both genotypes were grown in short day for 19 days and the roots and hypocotyls were dissected out when harvested. The process of RNA isolation, reverse transcription and quantitative PCR was described previously *(15).* The primers for qPCR are: *HAM1*: 5'-CGTCGTCAACATCAGTTTCAGTTTCC -3'and 5'-GATGTGAGAAGCTGCTCTTTGA -3'; *CLV3*: 5'-CAAGACAGCCAAGAAACAACTTT -3' and 5'-TCACTTCAGCAACAAACGTAATG -3'; and *UBC* (as the internal control): 5'-TGGACCGCTCTTATCAAAGGACC -3', and 5'-GCTCAGGATGAGCCATCAATGCT -3'.

Confocal imaging and image analysis

All of the fluorescent reporters were live-imaged by using a Zeiss LSM780 or a Zeiss LSM880 confocal microscope. The live-imaging experiments were performed as previously described *(15, 31)*. Each image result shown in the figures has been confirmed by at least four biological replicates. To image YPET, TFP and propidium iodide (PI) simultaneously from either *pHAM1::2xYPET-N7MirS*; *pCLV3::TFP-ER* SAMs or *pHAM2::YPET-HAM2*; *pCLV3::TFP-ER* SAMs, YPET was excited using a 543 nm laser line; PI was excited using a 514nm laser line; and the TFP was excited using 458 nm laser line. To image GFP and PI simultaneously in the *pATML1::HAM1m-GFP*; *pCLV3::DsRed-N7* SAMs, GFP was excited using a 488 nm laser line and PI was excited using a 514 nm laser line. To image DsRed and PI simultaneously in either *pCLV3::DsRed-N7* or *pATML1::HAM1m-GFP*; *pCLV3::DsRed-N7* SAMs, DsRed was excited using a 561 nm laser line and PI was excited using a 514 nm laser line. The quantification of confocal images (in Fig. 1-2, Fig. S1) was performed by using Fiji with the Fire selection in the LUT (Look up table) function.

RNA *in situ* hybridization and histological analysis

All of the plants for the RNA *in situ* hybridization in the SAMs and the histological analysis were grown under short day conditions (8 hour light /16 hour dark cycle) at 22 °C. For *in situ* hybridization, vegetative shoots were fixed, embedded, sectioned, hybridized and washed as described previously *(32, 33)* except for a hybridization temperature of 53 °C and no RNase A treatment after hybridization. The full length coding sequence of *CLV3*, *WUS* and *HAM1* were used as probes. Each RNA *in situ* hybridization experiment described was independently repeated at least two or three

times. Each *in situ* hybridization image shown in the main or supplementary figures has been confirmed through more than three biological replicates in total.

CLV3 RNA *in situ* hybridization was performed for the validation of the model predictions. For the direct comparison of the *CLV3* patterns in different genotypes, the plant samples of L*er* wild type, *ham1;2;3*, *wus-7*, or *wus-7;ham1;2;3* (in Fig. 3E-H) were grown in the same conditions, fixed at the same time (30 days after germination, DAG), and assayed identically; the plant samples of L*er* wild type, *ham1;2;3*, *wus-1*, or *wus-1;ham1;2;3* (in Fig. 3M-P) were grown in the same conditions, fixed at the same time (22 DAG), and assayed identically; the plant samples of L*er* wild type, *ham1;2;3*, *wus-1*, or *wus-1;ham1;2;3* (in Fig. S7) were grown in the same conditions, fixed at the same time (31 DAG), and assayed identically; the plant samples of wild type controls and *Mir171OE* plants (in Fig. S6) were grown in the same conditions, fixed at the same time (24 DAG), and assayed identically; and the plant samples of wild type and *ham1;2;3* (in Fig. 4) were grown in the same conditions, fixed at the same time (31 DAG), and assayed identically.

WUS RNA *in situ* hybridization was also performed for the validation of the model predictions. For direct comparisons of the *WUS* patterns during AM initiation, wild type and *ham1;2;3* plants (in Fig. S8) were grown in short days, then transferred to continuous light for 3 days before fixation, fixed at the same time, and assayed identically.

HAM1 RNA *in situ* hybridization was performed to determine the patterns of *HAM1* at different developmental stages during AM initiation (as model input). Wild type plants (in Fig. 4) were grown in short days then transferred to continuous light for 3-5 days for the induction of AM formation at different stages, prior to fixation.

RNA *in situ* hybridization with all sense probe controls was included (in Fig. S9) to validate the specificity of the experimental system. For each gene (*CLV3*, *WUS* and *HAM1*), the plant samples were harvested at the same time, and the *in situ* hybridization experiment was performed identically for either antisense probe or the sense probe control.

Quantitative measurement of *in situ* images (in Fig. S6A-B) from orthogonal sections through the middle of SAMs of six L*er* wild type and eleven *Mir171OE* samples was performed by using Fiji. Three parameters were quantified including the total signal intensity (pixel x intensity /pixel) that indicates if the *CLV3* mRNA level is increased (Fig. S6D), the area of positive signal (μm^2) that indicates if more cells express *CLV3* (Fig. S6E), and the distance from the center of positive signal area to the epidermis (μm) that reflects the apical-basal pattern of *CLV3* mRNA (Fig. S6F) in the SAMs.

For histological staining, vegetative shoots were fixed and embedded as for *in situ* hybridization. Sections were de-paraffinated, rehydrated, stained with 0.01% toluidine blue solution for 3 min, and rinsed with water. The plant samples of wild type and *pATML1::HAM1m-GFP*; *pCLV3::DsRed-N7* plants (in Fig. S5) were grown in the same conditions in short day and fixed at the same time (37 DAG).

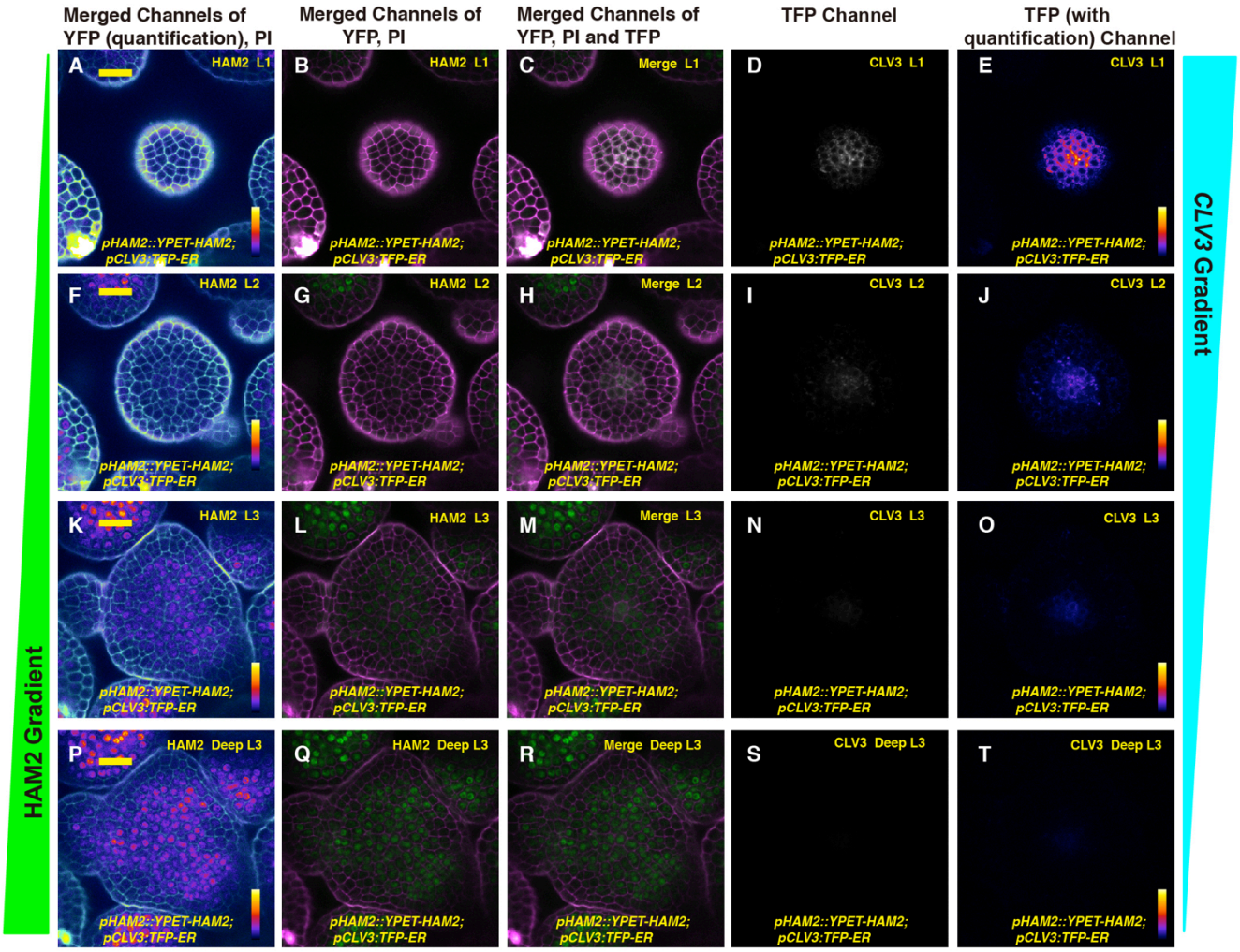

Fig. S1.

Nearly complementary expression patterns of HAM2 and *CLV3* in the SAM. Expression of *pHAM2::YPET-HAM2* and *pCLV3::TFP-ER* in transverse sections from top to bottom throughout the same *Arabidopsis* SAM, including L1 (A-E), L2 (F-J), the layer below the L2 (K-O) and deeper layers (P-T). Panels (from left to right): YFP (quantification indicated by color) and PI counter stain (white); YFP (green) and PI counter stain (purple); merged three channels of YFP (green), PI (purple) and TFP (gray); TFP (gray) channel; and TFP (quantification indicated by color). Scale bar (A-T): 20 µm; color bar: fire quantification of signal intensity.

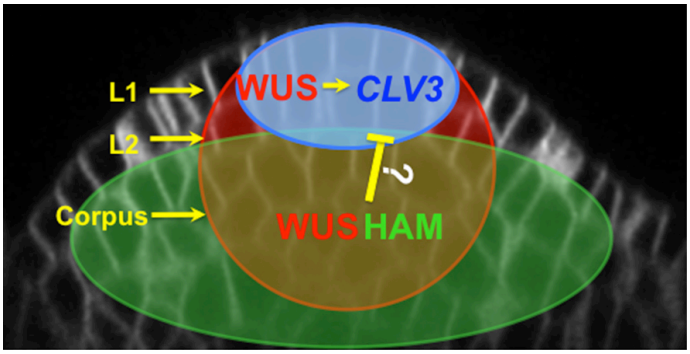

Fig. S2.
Summary of the expression domains of *CLV3* RNA (blue), WUS protein (red) and HAM (protein and RNA, green) in a SAM. The proposed regulatory circuit in control of stem cell dynamics is also summarized. The expression patterns of *HAM* and *CLV3* are largely complementary and *HAM1* (and *HAM2*) is co-expressed with *WUS* at the center of the rib meristem. WUS protein moves symplastically from the rib meristem to the upper two meristem cell layers (L1 and L2) to activate *CLV3* transcription (represented by arrow), and CLV3 peptide (which moves apoplastically) serves as a signal that restricts *WUS* transcript to the rib meristem. Different from the WUS protein, no movement of HAM protein from corpus to stem cells is detected. These facts are consistent with a hypothesis that in the central zone in the L1 and L2 layers where HAM is absent, WUS is able to activate *CLV3* transcription; beneath the central zone where HAM is present, HAM represses and/or HAM and WUS together do not activate *CLV3* transcription (with repressive interactions or absence of activation) (represented by bar). Consequently, the *CLV3* domain is established at the top of the SAM, dictating stem cell homeostasis during meristem development. L1, L2 and corpus indicate different cell layers.

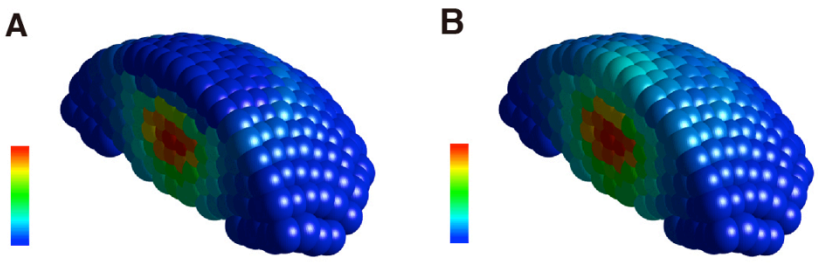

Fig. S3.
The *CLV3* expression domain in a wild type SAM cannot be reproduced *in silico* if we discard the hypothesis that the HAM abolishes the ability of WUS to activate *CLV3* mRNA production.

$$\frac{d[CLV3r]}{dt} = k_{crp}[WUSp][HAMp]\left(1 - \frac{[CLV3r]}{[CLV3r]_{max}}\right) - k_{crn}[CLV3r] \ldots\ldots\ldots\ldots\ldots\ldots\ldots\ldots (S3A)$$

$$\frac{d[CLV3r]}{dt} = k_{crp}[WUSp](1 + [HAMp])\left(1 - \frac{[CLV3r]}{[CLV3r]_{max}}\right) - k_{crn}[CLV3r] \ldots\ldots\ldots\ldots\ldots (S3B)$$

Equation S3A assumes that WUS and HAM work together to activate the production of *CLV3* mRNA (both HAM and WUS are required for the activation). Equation S3B assumes that HAM activates *CLV3* mRNA production in addition to WUS. From the mathematical perspective, these two scenarios and our hypothesis are equally possible, and from the biological perspective, these two possibilities have not been experimentally tested prior to the work here. Failure of these two hypothetical possibilities in model simulation: When Equation 3 was replaced with either Equation S3A or Equation S3B in the model, the simulated *CLV3* mRNA patterns (A and B) are different from the experimentally observed *CLV3* mRNA pattern. (A) The simulated *CLV3* mRNA expression domain in a wild-type SAM from the model using Equation S3A. Relative *CLV3* mRNA levels in each individual cell in different cell layers are indicated by color, with a gradient from red (maximum, 1.21 arbitrary units (a.u.)) to blue (none). (B) The simulated *CLV3* RNA domain is in a wild type SAM from the model using Equation S3B. Relative *CLV3* mRNA levels in each individual cell in different cell layers are indicated by color, with a gradient from red (maximum, 1.58 a.u.) to blue (none).

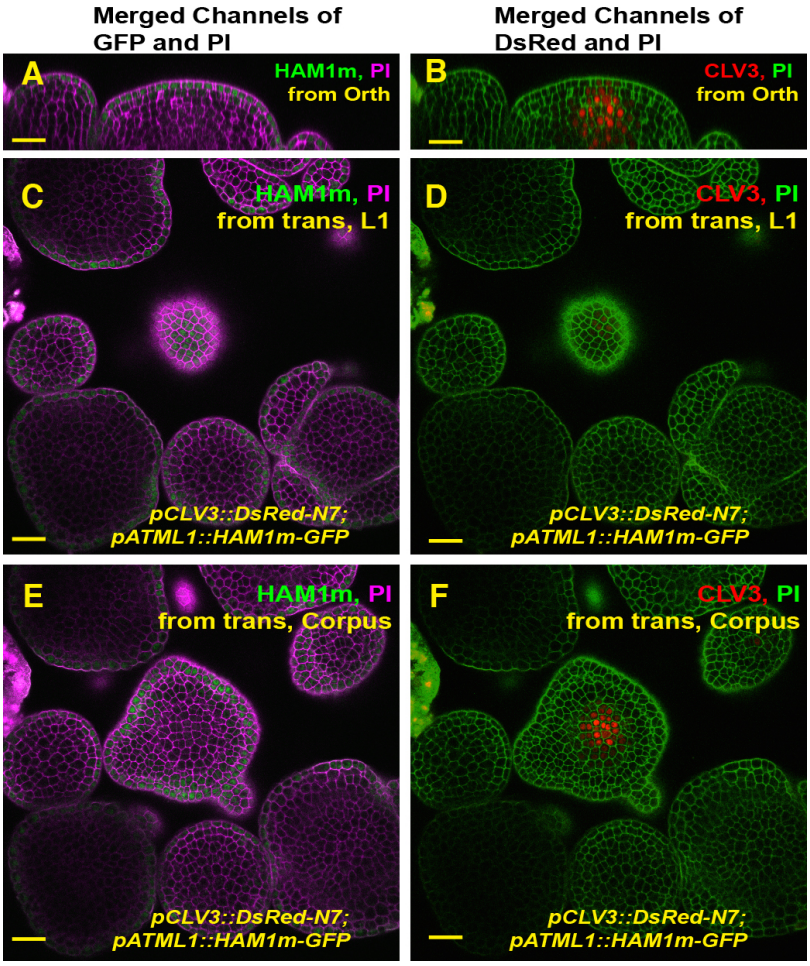

Fig. S4.
Confocal imaging of a *pATML1::HAM1m-GFP; pCLV3::DsRed-N7* SAM, including both orthogonal (A-B) and transverse (C-F) views. Left panels (A, C, E): merged channels from GFP (Green) and PI (Purple); Right panels (B, D, F): merged channels from DsRed (Red) and PI (Green). Scale bar (A-F): 25 μm.

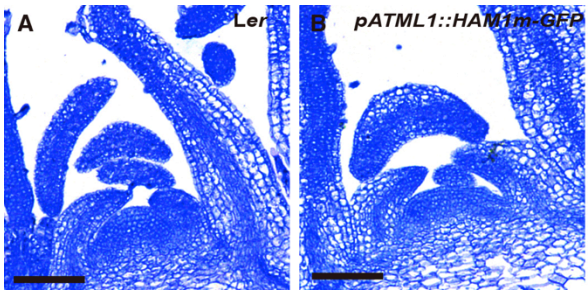

Fig. S5.
Orthogonal sections of SAMs from both L*er* wild type (A) and *pATML1::HAM1m-GFP* plant (B) at the same developmental stage grown in the same condition (at 37 DAG), demonstrating the enlarged SAM of *pATML1::HAM1m-GFP* plants compared to wild type. Scale bar: 100 µm.

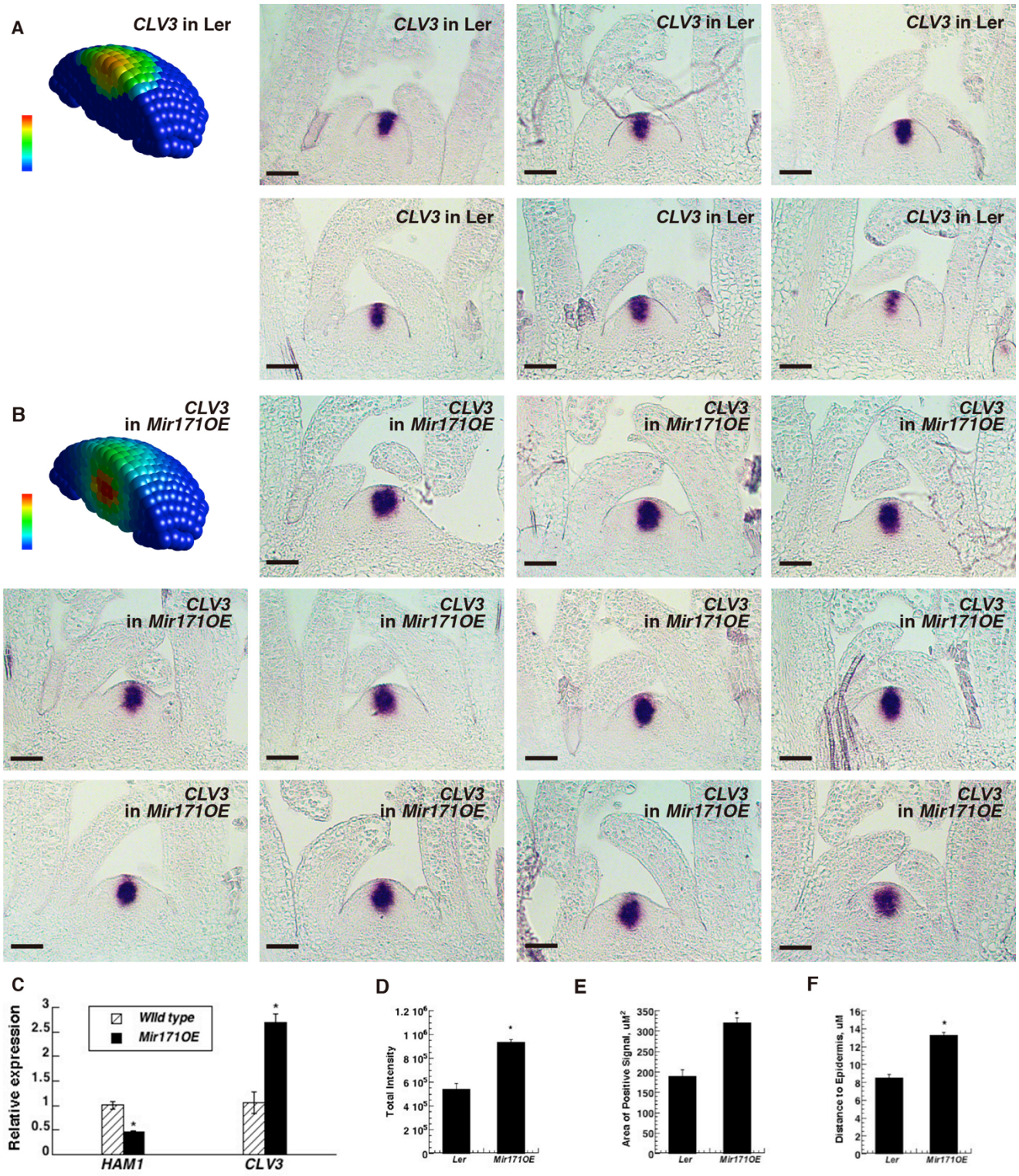

Fig. S6.
Model prediction, experimental validation and quantification of *CLV3* polarity upon the repression of *HAM* activity. (A-B) The simulated *CLV3* RNA expression domain in 3D in both wild type (first panel in A) and in a *Mir171* overexpressing (*Mir171OE*) transgenic

plant (first panel in B) in which *HAM1* is downregulated to around the 40% of the wild-type level. The simulated *CLV3* mRNA levels in each individual cell at different cell layers are indicated by color, with the gradient from red (maximum,1.02 a.u.) to blue (none). (A-B) Validation of the computational simulation through RNA *in situ* hybridization of *CLV3* in wild type SAMs (panels 2-7 in A) or in SAMs from the *Mir171OE* transgenic plants (panels 2-12 in B). All individual samples were fixed at the same developmental stage (24 DAG) and assayed under the same experimental conditions. Scale bar: 50 μm. (C) RT-PCR quantification of both *HAM1* and *CLV3* expression in *Mir171OE* compared to the wild type control. Error bar: SE calculated from three independent biological replicates. Stars: $P< 0.05$ (t-test). (D-F) Quantification of *CLV3* patterns in six L*er* wild type SAMs and eleven *Mir171OE* SAMs shown in (A-B), including the total intensity (pixel x average intensity/pixel, D), the area of positive signal (μm^2, E), and the distance from the center of positive area to epidermis (μm, F). Bars (D-F): Mean $\pm$ SE; Stars (D-F): $P<0.001$ (t-test).

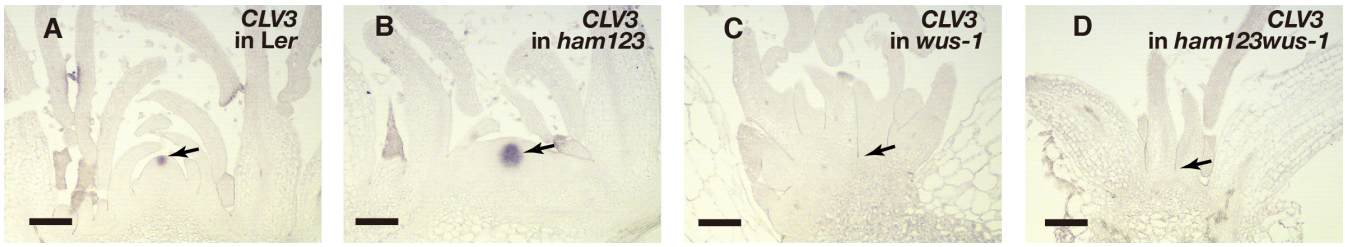

Fig. S7.
Validation of the simulation by RNA *in situ* hybridization of *CLV3* in the SAM of wild type (L*er*) (A), *ham1;2;3* (B), *wus-1* (C), and *wus-1; ham1;2;3* (D) at 31 DAG under the same experimental conditions. Arrows indicate *CLV3*-expressing cells in the meristems (A-B) and they indicate no *CLV3* expression in (C-D). Scale bar: 200 µm.

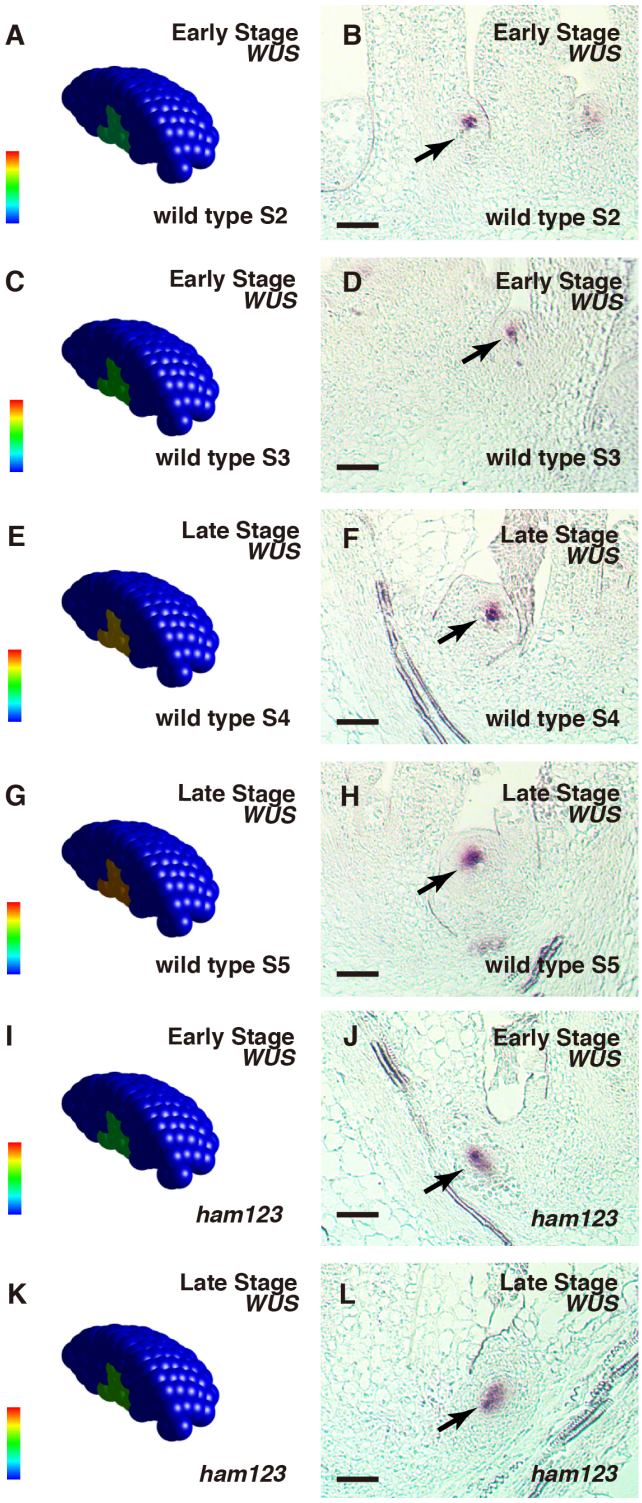

Fig. S8.
The patterns of *WUS* expression during axillary meristem initiation. Model prediction and experimental validation of *WUS* RNA patterns during the *de novo* formation of new stem cell niches in wild type (A-H) and in the *ham1;2;3* mutant (I-L). (A, C, E, G) Simulated *WUS* mRNA levels at early stages (A, C) and late stages (E, G) in wild type. (B, D, F, H) Validation of *WUS* mRNA patterns through RNA *in situ* hybridization to wild type at

early (B, D) and late stages (F, H) of AM initiation. (I, K) Simulated *WUS* mRNA levels at both early and late stages in *ham1;2;3* and (J, L) Validation of the simulation through RNA *in situ* hybridization of *ham1;2;3* AMs at both early (J) and late (L) stages. The initiation of AMs in the *ham1;2;3* mutant was significantly disturbed, did not follow the well-characterized developmental stages *(23-24).* The early stage (J) and late stage (L) of AM initiation in the same *ham1;2;3* plant were defined based on the distance of leaf axils from the main SAM in longitudinal sections. (A, C, E, G, I, K) Relative *WUS* mRNA levels (as the output) in each individual cell are also indicated by color (blue is no expression, and red is expression at 1.23 a.u.). Arrows indicate *WUS*-expressing cells during new meristem initiation. Scale bar: 50 μm.

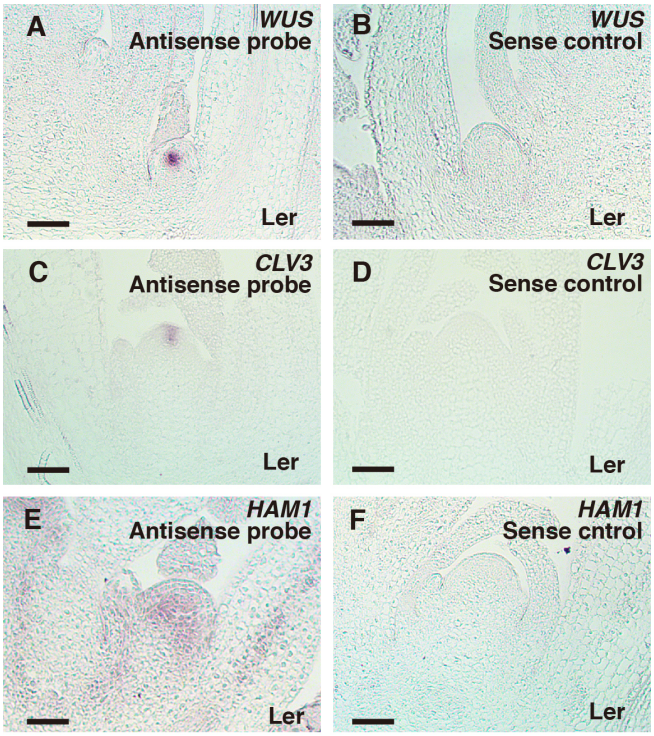

Fig. S9.
Sense probe controls for RNA *in situ* experiments. (A-B) RNA *in situ* hybridization of *WUS* in wild type AMs using either antisense probe (A) or a sense probe control (B). (C-D) RNA *in situ* hybridization of *CLV3* in wild type AMs using either antisense probe (C) or a sense probe control (D). (E-F) RNA *in situ* hybridization to *HAM1* RNA in wild type AMs using either antisense probe (E) or the sense probe control (F). For assaying each RNA (*CLV3*, *WUS* or *HAM1*), the plant samples were harvested at the same time, and the *in situ* hybridization experiment was performed identically for either antisense probe or sense probe control. Scale bar: 50 µm.

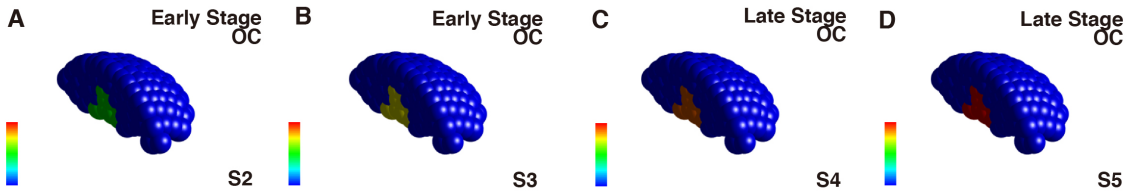

Fig. S10.

(A-D) The level of OC signal at early (A-B) and late stages (C-D) as the input for the simulation during new meristem initiation. Relative OC level in each individual cell in different cell layers is indicated by color, with a gradient from red (maximum, 1 a.u.) to blue (none).

Parameter	Biological Meaning	Value	Unit
k_{wrp}	Parameter for *WUS* mRNA production	0.4	/h
$[WUSr]_{max}$	Maximum *WUS* mRNA level	3	a.u.
k_{wrn}	General parameter for *WUS* mRNA degradation	0.8	/h
γ_{WUSr}	Parameter for CLV3 independent *WUS* mRNA degradation	0.1	a.u.
k_{wpp}	Parameter for WUS protein translation	1	/h
k_{wpn}	Parameter for WUS protein degradation	0.3	/h
D_{WUSp}	Passive diffusion-like symplastic transport rate of WUS protein	0.05	a.u. of area/h
k_{crp}	Parameter for *CLV3* mRNA production	2	/h
$[CLV3r]_{max}$	Maximum *CLV3* mRNA level	3	a.u.
k_{crn}	Parameter for *CLV3* mRNA degradation	0.4	/h
k_{cpp}	Parameter for CLV3 peptide production	2.5	/h
k_{cpn}	Parameter for CLV3 peptide degradation	0.3	/h
D_{CLV3p}	Passive diffusion-like apoplastic transport rate of CLV3 peptide	0.3	a.u. of area/h
$C_{bufferlow}$	Low threshold of the buffered range of *CLV3* mRNA	0.15	a.u.
$C_{bufferhigh}$	High threshold of the buffered range of *CLV3* mRNA	1.44	a.u.

Table S1.
Parameters settings for SAM model.

Movie S1
Full stacks of confocal image sections of the *HAM1* reporter (green) in the same wild type SAM as in Fig. 1, with cellular outlines (gray) stained with propidium iodide (PI), from the bottom to the top, showing the apical-basal gradient of *HAM1* expression.

Movie S2
Full stacks of confocal image sections of the *CLV3* reporter (cyan) in the same wild type SAM shown in Movie S1 with cellular outlines (gray) stained with propidium iodide (PI), from the bottom to the top, showing the apical-basal gradient of *CLV3* expression.

Movie S3
Full stacks of confocal image sections of both *HAM1* reporter (green) and *CLV3* reporter (cyan) in the same wild type SAM shown in Movie S1 and Movie S2 with cellular outlines (gray) stained with propidium iodide (PI), from the bottom to the top. It shows that the expression patterns of *HAM1* and *CLV3* are largely complementary along the apical-basal axis, with opposite concentration gradients.

Movie S4
Simulation for *WUS* transcript levels in a wild type SAM during meristem development over 72 hours with growth and cell divisions. We assume that on average, cells divide every 24 hours. The WUS mRNA expression domain stays stable in the simulated time course. Relative levels of *WUS* mRNA are shown using arbitrary units, with a gradient from red (maximum, 1.1229 a.u.) to blue (none).

Movie S5
Simulation for WUS protein levels in a wild type SAM during meristem development over 72 hours with growth and cell divisions. The WUS protein expression domain stays stable in the simulated time course. Relative level of WUS protein is shown using arbitrary units, with a gradient from red (maximum, 0.949 a.u.) to blue (none).

Movie S6
Simulation for *CLV3* transcript levels in a wild type SAM during meristem development over 72 hours with growth and cell divisions. The *CLV3* mRNA expression domain stays stable in the simulated time course. Relative level of *CLV3* mRNA is described using arbitrary units, with a gradient from red (maximum, 0.8621 a.u.) to blue (none).

Movie S7
Simulation for *WUS* and *CLV3* transcript levels in a simplified one dimensional wild type SAM from null initial levels (at 0 h) to steady state levels (at 48 h). Relative levels of *WUS* and *CLV3* mRNA are shown using normalized arbitrary values (from 0 to 1 normalized according to their respective maximum steady state levels). Red color indicates high expression level (1) and blue color indicates no expression.

Movie S8

Simulation for *WUS* transcript levels in a wild type SAM from null initial level (at 0 h) to steady state levels (at 48 h). Red color indicates high expression level (1.1229 a.u.) and blue color indicates no expression (0).

Movie S9
Simulation for *CLV3* transcript levels in a wild type SAM from null initial level (at 0 h) to steady state levels (at 48 h). Red color indicates high expression level (0.8621 a.u.) and blue color indicates no expression (0).

Movie S10
Full stacks of confocal image sections of the *pATML1::HAM1m-GFP* reporter (green) in the same *pATML1::HAM1m-GFP; pCLV3::DsRed-N7* SAM as shown in Fig. S4, with cellular outlines (purple) stained with propidium iodide (PI), from the bottom to the top.

Movie S11
Full stacks of confocal image sections of the *pCLV3::DsRed-N7* reporter (red) in the same *pATML1::HAM1m-GFP; pCLV3::DsRed-N7* SAM as shown in Fig. S4, with cellular outlines (green) stained with propidium iodide (PI), from the bottom to the top, showing that the expression *CLV3* at L1 is dramatically reduced when HAM1m-GFP is expressed at L1.

Movie S12
Simulation for *CLV3* transcript levels in a wild type AM from early to late developmental stages. Red color indicates the expression levels at or above 0.61 a.u., and blue color indicates no expression (0).

Movie S13
Simulation for *CLV3* transcript levels in a *ham1;2;3* mutant AM from early to late developmental stages. Red color indicates high expression level (1.2316 a.u.) and blue color indicates no expression (0).

Movie S14
Simulation for *WUS* transcript levels in a wild type AM from early to late developmental stages. Red color indicates the expression levels at or above 0.61 a.u., and blue color indicates no expression (0).

Movie S15
Simulation for *WUS* transcript levels in a *ham1;2;3* mutant AM from early to late developmental stages. Red color indicates the expression levels at or above 0.61 a.u., and blue color indicates no expression (0).

References and Notes

1. E. M. Meyerowitz, Genetic control of cell division patterns in developing plants. *Cell* **88**, 299–308 (1997). doi:10.1016/S0092-8674(00)81868-1 Medline

2. J. C. Fletcher, U. Brand, M. P. Running, R. Simon, E. M. Meyerowitz, Signaling of cell fate decisions by *CLAVATA3* in *Arabidopsis* shoot meristems. *Science* **283**, 1911–1914 (1999). doi:10.1126/science.283.5409.1911 Medline

3. U. Brand, J. C. Fletcher, M. Hobe, E. M. Meyerowitz, R. Simon, Dependence of stem cell fate in *Arabidopsis* on a feedback loop regulated by *CLV3* activity. *Science* **289**, 617–619 (2000). doi:10.1126/science.289.5479.617 Medline

4. U. Brand, M. Grünewald, M. Hobe, R. Simon, Regulation of *CLV3* expression by two homeobox genes in Arabidopsis. *Plant Physiol.* **129**, 565–575 (2002). doi:10.1104/pp.001867 Medline

5. T. Laux, K. F. Mayer, J. Berger, G. Jürgens, The WUSCHEL gene is required for shoot and floral meristem integrity in Arabidopsis. *Development* **122**, 87–96 (1996). Medline

6. K. F. Mayer, H. Schoof, A. Haecker, M. Lenhard, G. Jürgens, T. Laux, Role of *WUSCHEL* in regulating stem cell fate in the *Arabidopsis* shoot meristem. *Cell* **95**, 805–815 (1998). doi:10.1016/S0092-8674(00)81703-1 Medline

7. H. Schoof, M. Lenhard, A. Haecker, K. F. X. Mayer, G. Jürgens, T. Laux, The stem cell population of *Arabidopsis* shoot meristems in maintained by a regulatory loop between the *CLAVATA* and *WUSCHEL* genes. *Cell* **100**, 635–644 (2000). doi:10.1016/S0092-8674(00)80700-X Medline

8. Z. L. Nimchuk, P. T. Tarr, C. Ohno, X. Qu, E. M. Meyerowitz, Plant stem cell signaling involves ligand-dependent trafficking of the CLAVATA1 receptor kinase. *Curr. Biol.* **21**, 345–352 (2011). doi:10.1016/j.cub.2011.01.039 Medline

9. Z. L. Nimchuk, Y. Zhou, P. T. Tarr, B. A. Peterson, E. M. Meyerowitz, Plant stem cell maintenance by transcriptional cross-regulation of related receptor kinases. *Development* **142**, 1043–1049 (2015). doi:10.1242/dev.119677 Medline

10. R. K. Yadav, M. Perales, J. Gruel, T. Girke, H. Jönsson, G. V. Reddy, WUSCHEL protein movement mediates stem cell homeostasis in the *Arabidopsis* shoot apex. *Genes Dev.* **25**, 2025–2030 (2011). doi:10.1101/gad.17258511 Medline

11. G. Daum, A. Medzihradszky, T. Suzaki, J. U. Lohmann, A mechanistic framework for noncell autonomous stem cell induction in *Arabidopsis*. *Proc. Natl. Acad. Sci. U.S.A.* **111**, 14619–14624 (2014). doi:10.1073/pnas.1406446111 Medline

12. M. Perales, K. Rodriguez, S. Snipes, R. K. Yadav, M. Diaz-Mendoza, G. V. Reddy, Threshold-dependent transcriptional discrimination underlies stem cell homeostasis. *Proc. Natl. Acad. Sci. U.S.A.* **113**, E6298–E6306 (2016). doi:10.1073/pnas.1607669113 Medline

13. H. Jönsson, M. Heisler, G. V. Reddy, V. Agrawal, V. Gor, B. E. Shapiro, E. Mjolsness, E. M. Meyerowitz, Modeling the organization of the *WUSCHEL* expression domain

in the shoot apical meristem. *Bioinformatics* **21**, i232–i240 (2005). doi:10.1093/bioinformatics/bti1036 Medline

14. J. Gruel, B. Landrein, P. Tarr, C. Schuster, Y. Refahi, A. Sampathkumar, O. Hamant, E. M. Meyerowitz, H. Jönsson, An epidermis-driven mechanism positions and scales stem cell niches in plants. *Sci. Adv.* **2**, e1500989 (2016). doi:10.1126/sciadv.1500989 Medline

15. Y. Zhou, X. Liu, E. M. Engstrom, Z. L. Nimchuk, J. L. Pruneda-Paz, P. T. Tarr, A. Yan, S. A. Kay, E. M. Meyerowitz, Control of plant stem cell function by conserved interacting transcriptional regulators. *Nature* **517**, 377–380 (2015). doi:10.1038/nature13853 Medline

16. S. Schulze, B. N. Schäfer, E. A. Parizotto, O. Voinnet, K. Theres, *LOST MERISTEMS* genes regulate cell differentiation of central zone descendants in Arabidopsis shoot meristems. *Plant J.* **64**, 668–678 (2010). doi:10.1111/j.1365-313X.2010.04359.x Medline

17. E. M. Engstrom, C. M. Andersen, J. Gumulak-Smith, J. Hu, E. Orlova, R. Sozzani, J. L. Bowman, Arabidopsis homologs of the *Petunia HAIRY MERISTEM* gene are required for maintenance of shoot and root indeterminacy. *Plant Physiol.* **155**, 735–750 (2011). doi:10.1104/pp.110.168757 Medline

18. L. Wang, Y. X. Mai, Y. C. Zhang, Q. Luo, H. Q. Yang, MicroRNA171c-targeted *SCL6-II*, *SCL6-III*, and *SCL6-IV* genes regulate shoot branching in *Arabidopsis*. *Mol. Plant* **3**, 794–806 (2010). doi:10.1093/mp/ssq042 Medline

19. R. Müller, L. Borghi, D. Kwiatkowska, P. Laufs, R. Simon, Dynamic and compensatory responses of *Arabidopsis* shoot and floral meristems to *CLV3* signaling. *Plant Cell* **18**, 1188–1198 (2006). doi:10.1105/tpc.105.040444 Medline

20. P. Lu, R. Porat, J. A. Nadeau, S. D. O'Neill, Identification of a meristem L1 layer-specific gene in Arabidopsis that is expressed during embryonic pattern formation and defines a new class of homeobox genes. *Plant Cell* **8**, 2155–2168 (1996). doi:10.1105/tpc.8.12.2155 Medline

21. C. Llave, Z. Xie, K. D. Kasschau, J. C. Carrington, Cleavage of *Scarecrow-like* mRNA targets directed by a class of *Arabidopsis* miRNA. *Science* **297**, 2053–2056 (2002). doi:10.1126/science.1076311 Medline

22. P. Graf, A. Dolzblasz, T. Würschum, M. Lenhard, U. Pfreundt, T. Laux, *MGOUN1* encodes an *Arabidopsis* type IB DNA topoisomerase required in stem cell regulation and to maintain developmentally regulated gene silencing. *Plant Cell* **22**, 716–728 (2010). doi:10.1105/tpc.109.068296 Medline

23. J. Long, M. K. Barton, Initiation of axillary and floral meristems in *Arabidopsis*. *Dev. Biol.* **218**, 341–353 (2000). doi:10.1006/dbio.1999.9572 Medline

24. W. Xin, Z. Wang, Y. Liang, Y. Wang, Y. Hu, Dynamic expression reveals a two-step patterning of *WUS* and *CLV3* during axillary shoot meristem formation in *Arabidopsis*. *J. Plant Physiol.* **214**, 1–6 (2017). doi:10.1016/j.jplph.2017.03.017 Medline

25. V. S. Chickarmane, S. P. Gordon, P. T. Tarr, M. G. Heisler, E. M. Meyerowitz, Cytokinin signaling as a positional cue for patterning the apical-basal axis of the growing *Arabidopsis* shoot meristem. *Proc. Natl. Acad. Sci. U.S.A.* **109**, 4002–4007 (2012). doi:10.1073/pnas.1200636109 Medline

26. J. Gruel, J. Deichmann, B. Landrein, T. Hitchcock, H. Jönsson, A model of protein interactions for regulating plant stem cells. bioRxiv 237933 [Preprint]. 21 December 2017. https://doi.org/10.1101/237933.

27. G. V. Reddy, M. G. Heisler, D. W. Ehrhardt, E. M. Meyerowitz, Real-time lineage analysis reveals oriented cell divisions associated with morphogenesis at the shoot apex of *Arabidopsis thaliana*. *Development* **131**, 4225–4237 (2004). doi:10.1242/dev.01261 Medline

28. A. Cunha, P. T. Tarr, A. H. K. Roeder, A. Altinok, E. Mjolsness, E. M. Meyerowitz, Computational analysis of live cell images of the *Arabidopsis thaliana* plant. *Methods Cell Biol.* **110**, 285–323 (2012). doi:10.1016/B978-0-12-388403-9.00012-6 Medline

29. S. J. Clough, A. F. Bent, Floral dip: A simplified method for *Agrobacterium*-mediated transformation of *Arabidopsis thaliana*. *Plant J.* **16**, 735–743 (1998). doi:10.1046/j.1365-313x.1998.00343.x Medline

30. A. H. Roeder, A. Cunha, C. K. Ohno, E. M. Meyerowitz, Cell cycle regulates cell type in the *Arabidopsis* sepal. *Development* **139**, 4416–4427 (2012). doi:10.1242/dev.082925 Medline

31. W. Li, Y. Zhou, X. Liu, P. Yu, J. D. Cohen, E. M. Meyerowitz, LEAFY controls auxin response pathways in floral primordium formation. *Sci. Signal.* 6, ra23 (2013). doi:10.1126/scisignal.2003937

32. X. Zhang, Y. Zhou, L. Ding, Z. Wu, R. Liu, E. M. Meyerowitz, Transcription repressor HANABA TARANU controls flower development by integrating the actions of multiple hormones, floral organ specification genes, and GATA3 family genes in *Arabidopsis*. *Plant Cell* **25**, 83–101 (2013). doi:10.1105/tpc.112.107854 Medline

33. B. A. Krizek, Ectopic expression of *AINTEGUMENTA* in *Arabidopsis* plants results in increased growth of floral organs. *Dev. Genet.* **25**, 224–236 (1999). doi:10.1002/(SICI)1520-6408(1999)25:3<224:AID-DVG5>3.0.CO;2-Y Medline